Vibronic structure in C_2H and C_2D from anion slow electron velocity-map imaging spectroscopy

Jia Zhou and Etienne Garand
Department of Chemistry, University of California, Berkeley, California 94720, USA

Daniel M. Neumark[a)]
Department of Chemistry, University of California, Berkeley, California 94720, USA and Chemical Sciences Division, Lawrence Berkeley National Laboratory, Berkeley, California 94720, USA

(Received 6 June 2007; accepted 13 July 2007; published online 20 September 2007)

The C_2H and C_2D radicals are investigated by slow electron velocity-map imaging (SEVI) of the corresponding anions. This technique offers considerably higher resolution (<0.5 meV) than photoelectron spectroscopy. As a result, SEVI spectra of the two isotopomers yield improved electron affinities and reveal many new structures that are particularly sensitive to vibronic coupling between the ground $^2\Sigma^+$ and low-lying excited $^2\Pi$ states. These structures, which encompass more than 5000 cm^{-1} of internal excitation, are assigned with the aid of previous experimental and theoretical work. We also show that SEVI can be applied to photodetachment transitions resulting in ejection of an electron with orbital angular momentum $l=1$, a p wave, in contrast to anion zero-electron kinetic energy spectroscopy which is restricted to s-wave detachment. © *2007 American Institute of Physics*. [DOI: 10.1063/1.2768932]

I. INTRODUCTION

This paper focuses on the spectroscopy of the ethynyl radical C_2H using the recently developed anion photodetachment technique of slow electron velocity-map imaging (SEVI).[1] One of the smallest carbon monohydrides, the ethynyl radical has been observed in abundance among various interstellar mediums[2–8] and is an important reactive intermediate in combustion processes.[9–11] Numerous spectroscopic techniques have been applied to this radical, including electron spin resonance,[12–14] laser magnetic resonance,[15–18] microwave and millimeter-wave spectroscopies,[19–23] matrix isolation infrared (IR) spectroscopy,[24–27] color center, difference-frequency and diode laser spectroscopies,[28–38] Fourier transform infrared emission spectroscopy,[39] laser-induced fluorescence,[40–42] and photoelectron (PE) spectroscopy of the C_2H^- anion.[43,44] Theoretical work on the spectroscopy of the radical has been carried out by Peyerimoff and co-workers,[45–52] and more recently, by Carter and co-workers.[53–55]

This extensive body of spectroscopic and theoretical work has shown that C_2H, a linear, triatomic species, is an important model system for understanding the interactions between close-lying electronic states in polyatomic molecules. C_2H exhibits a complex vibronic coupling in its ground state, owing to a conical intersection between the ground $\tilde{X}\,^2\Sigma^+(A')$ state and the low-lying $^2\Pi(A')$ and $^2\Pi(A'')$ states, which are about 3700 cm^{-1} above the ground state. Along the linear axis, there is Renner-Teller coupling between the electronic and vibrational angular momenta of the $^2A'$ and $^2A''$ components of the $^2\Pi$ state, while the bend vibration induces pseudo-Jahn-Teller coupling between the $^2\Sigma^+$ state and the $^2A'$ component of the $^2\Pi$ state.[54] The resulting breakdown of the Born-Oppenheimer approximation complicates vibrational assignments of the C_2H radical, and poses a challenge to both theory and experiment.

Much of our understanding of these effects in C_2H has come from rotationally resolved IR spectroscopy, but PE spectroscopy of C_2H^- has provided additional and complementary information. While IR spectroscopy probes transitions within the $^2\Sigma^+$ state and between the $\tilde{X}\,^2\Sigma^+$ and $\tilde{A}\,^2\Pi$ states, the selection rules in PE spectroscopy enable one to map out the ground and low-lying states of C_2H on an equal footing via photodetachment from the anion $\tilde{X}\,^1\Sigma^+$ ground state. In IR spectroscopy, one can infer the extent of vibronic coupling between the $^2\Sigma^+$ and $^2\Pi$ states for each band by determination of the effective spin-orbit coupling constant,[31,36] whereas in PE spectroscopy, vibronic coupling is evidenced by the observation of nominally forbidden transitions and anomalous photoelectron angular distributions.[56]

Ervin and Lineberger[43] measured the first photoelectron spectra of C_2H^- and C_2D^-. They observed a spectrum dominated by the $\tilde{X}\,^2\Sigma^+$-$\tilde{X}\,^1\Sigma^+$ 0-0 origin band, indicating a small geometry change between the anion and the radical ground state. The PE spectrum exhibited numerous transitions involving the bending (ν_2) and the C–C stretching (ν_3) modes. Vibronic coupling was manifested in the observation of odd $\Delta\nu_2$ transitions; such transitions in a non-totally symmetric vibration would otherwise have no intensity in one-photon photodetachment. Spectra taken at different laser polarizations showed that the odd $\Delta\nu_2$ transitions had a different photoelectron angular distribution than the even $\Delta\nu_2$ transi-

[a)]Author to whom correspondence should be addressed. Electronic mail: dneumark@berkeley.edu

tions. At the photon energy used in this experiment, 3.531 eV, the origin of the $\tilde{A}\,^2\Pi$ state was not observed.

PE spectra of C_2H^- and C_2D^- at 4.657 eV (266 nm) were reported by Taylor *et al.*[44] Strong transitions were observed in the region of the $\tilde{A}\,^2\Pi$ state origin, where overlapped transitions to the $\tilde{X}\,^2\Sigma^+$ and $\tilde{A}\,^2\Pi$ states were expected. Assignments were made based on previous experiments and the photoelectron angular distributions. The latter showed strong variations among the various peaks, and assignments relied on the reasoning that transitions to neutral levels with dominant $\tilde{A}\,^2\Pi$ state character would show different angular distributions than those primarily associated with the $\tilde{X}\,^2\Sigma^+$ state. Nonetheless, some of the assignments were problematic. In particular, based on the well known $\tilde{A}(010)$-$\tilde{X}(010)$ sequence-band in the IR spectrum,[29] one of the most intense features in the PE spectrum, lying 4155 cm^{-1} above the ground state origin in C_2H, was assigned to the forbidden transition from the anion ground vibrational state to the $\nu_2=1$ of the $\tilde{A}$ state with Σ^- symmetry $[\tilde{A}(01^-0)]$.

According to recent calculations by Tarroni and Carter,[54] the electronic origin of the $\tilde{A}$ state in the C_2H radical is actually spread over several vibronic levels around 4000 cm^{-1} above the origin of the $\tilde{X}$ state, suggesting that the above feature, as well as other peaks in the PE spectrum, are composed of multiple overlapping vibronic transitions. Such a complex spectrum, with vibronic levels separated by only a few meV, presents a challenge to anion PE spectroscopy, as its energy resolution is at best 5–10 meV. Hence, photodetachment spectra at higher resolution are needed to determine the extent to which overlapping transitions contributed to the PE spectrum, and to obtain improved assignments. While anion zero-electron kinetic energy (ZEKE) spectroscopy offers considerably higher resolution (0.1–0.3 meV),[57] it is a challenging and time-consuming experiment. Moreover, anion ZEKE experiments are limited to species where the photoelectrons leave as an *s* wave, with orbital angular momentum $l=0$. The SEVI technique[1] was developed in our laboratory with the goal of combining the advantage of PE spectroscopy with the resolving power of ZEKE.

Here, we present the SEVI spectra of C_2H^- and C_2D^- in order to gain new insights into non-adiabatic coupling in the ethynyl radical and to address issues left unresolved in earlier PE spectra. Many new features are resolved, particularly for C_2D, for which we mapped out several higher-lying energy levels that, to our knowledge, have not been observed previously in gas phase IR spectroscopy. In addition, we show that SEVI can be applied to photodetachment transitions that proceed by *p*-wave detachment.

II. EXPERIMENT

The SEVI apparatus has been described in detail elsewhere.[1,58,59] In SEVI, mass-selected anions are photodetached at a set wavelength. The resulting photoelectrons are collected via velocity-map imaging[60] (VMI) using relatively low extraction voltages, with the goal of selectively detecting slow electrons with high efficiency and enlarging their image on the detector. A series of images can be obtained at different wavelengths, each yielding a high-resolution photoelectron spectrum over a limited range of electron kinetic energy.

Briefly, C_2H^- (C_2D^-) anions were produced by expanding 100 psi (250 psi) of a mixture of 4% acetylene (acetylene-d_2), 48% carbon dioxide, and 48% argon into the source vacuum chamber through an Even-Lavie pulsed valve[61] equipped with a circular ionizer. Anions formed in the gas expansion were perpendicularly extracted into a Wiley-McLaren time-of-flight mass spectrometer and directed to the detachment region by a series of electrostatic lens and pinholes. A 1 μs pulse on the last ion deflector allowed only the desired mass into the interaction region. Anions were photodetached between the repeller and the extraction plates of the VMI stack by the focused output of a Nd:YAG pumped tunable dye laser. The photoelectron cloud formed was then coaxially extracted down a 50 cm flight tube and mapped onto a detector comprising a chevron-mounted pair of time-gated, imaging quality microchannel plates coupled to a phosphor screen, as is typically used in photofragment imaging experiments.[62] Events on the screen were collected by a 1024×1024 charge-coupled device (CCD) camera and sent to a computer. Electron velocity-mapped images resulting from 25 000–100 000 laser pulses were summed, quadrant symmetrized, and inverse-Abel transformed. Photoelectron spectra were obtained via angular integration of the transformed images.

The apparatus was calibrated by acquiring SEVI images of atomic chloride and iodide at several different photon energies for each repeller voltage used (150–350 V). At a radius of ~300 pixels, $\Delta E/E$ of 2% can be achieved. In the 150 V images, the full width at half maximum (FWHM) was 1.5 cm^{-1} at 10 cm^{-1} above threshold, while in the 350 V images the FWHM was 2.8 cm^{-1} at 23 cm^{-1} above threshold. Within the same image, all observed transitions have similar widths in pixels (Δr), which means that transitions observed further from threshold (larger r) are broader in energy. These effects are illustrated in Fig. 1, showing a transformed SEVI image of Cl^- taken at 350 V. The outer and inner rings correspond to photodetachment to the $Cl(^2P_{3/2})$ ground state and $Cl(^2P_{1/2})$ spin-orbit excited state, respectively. Both rings are about 2 pixels wide but the outer ring is considerably broader in energy.

Overall, by varying the laser wavelength and VMI voltages, the instrument can be operated in distinct modes, each with its own pros and cons. For example, operation at higher repeller voltages results in efficient collection of electrons over a wide kinetic energy range at lower resolution, while reducing the repeller voltage restricts efficient collection to lower energy electrons and yields higher resolution. In a similar vein, at a fixed repeller voltage, the resolution observed for a particular photodetachment transition will depend on how far the photon energy lies above the threshold for that transition, with the resolution improving as the photon energy is brought closer to threshold. However, at fixed wavelength, lower repeller voltages often result in poorer signal-to-noise ratio, as the image radius is larger and therefore spread over more pixels. Moreover, the photodetachment cross section drops close to threshold for all transitions

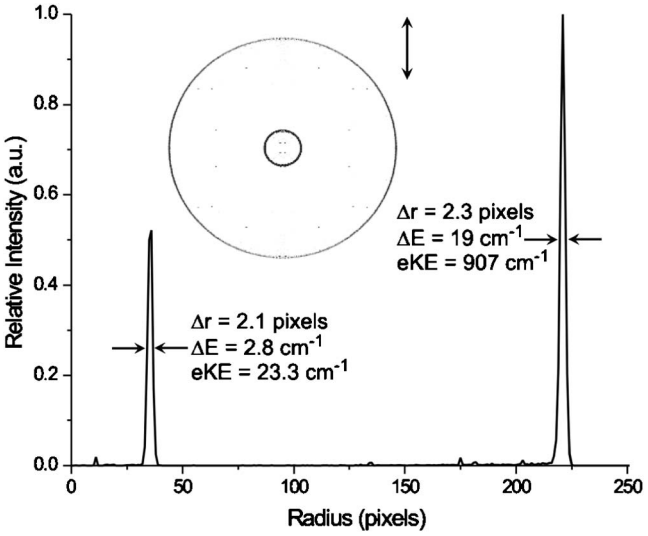

FIG. 1. SEVI image and specturm of atomic chloride plotted in pixels taken at a repeller voltage of 350 V. The outer and inner rings are transitions to the Cl $^2P_{3/2}$ and $^2P_{1/2}$ levels, respectively. The FWHM of the two features are similar in pixels, but the $^2P_{1/2}$ feature is narrower in energy.

(some much more than others, as discussed below), thus limiting how close one can operate to a particular threshold while maintaining an acceptable signal-to-noise ratio. The spectra presented in the following section are taken under operating conditions yielding reasonable resolution and signal-to-noise ratio, taking into account that the ultimate linewidth in SEVI of molecular anions is generally determined by unresolved rotational structure rather than instrumental limitations.

III. RESULTS AND ANALYSIS

SEVI spectra of C_2H^- taken at repeller voltages of 150–250 V are presented in Fig. 2, while SEVI spectra of C_2D^- taken at 250–350 V are shown in Fig. 3. The arrows in the spectra indicate the photon energies with which various images were taken. The spectra are plotted with respect to electron binding energy, *e*BE, the difference between the photon energy and the measured electron kinetic energy (*e*KE),

$$e\mathrm{BE} = h\nu - e\mathrm{KE}. \quad (1)$$

The top panels of Figs. 2 and 3 show the corresponding PE spectrum recorded by Taylor *et al.*[44] at 266 nm and a laser polarization angle of 55°, the "magic angle" (previously unpublished; Ref. 44 presents spectra taken at 0° and 90°). The SEVI spectra are presented in the four panels below, with regions I–IV indicated in the PE spectrum. Compared to the PE spectrum acquired by Taylor *et al.*,[44] it is clear that SEVI resolves many more transitions. The four regions do not overlap in energy, but spectra have been acquired for all intermediate energies, and no features in addition to those in Figs. 2 and 3 were seen. Many features were examined at higher resolution by taking their SEVI spectra closer to threshold (i.e., the gray trace in panel III, Fig. 2), and the peak widths given below are from such spectra. The relative intensities of the transitions in SEVI spectra change depending on the photon energy (detailed below); therefore, the

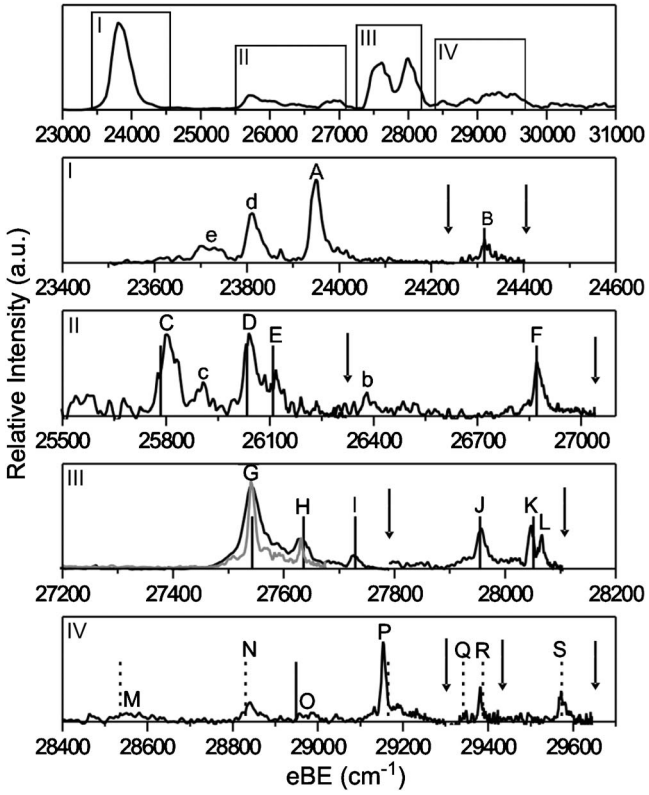

FIG. 2. SEVI spectra of C_2H^- in spectral regions I–IV. Top trace is the PE spectrum recorded by Taylor *et al.* (Ref. 44) at 55° laser polarization, with the corresponding regions I–IV indicated. The arrows indicate photon energies in the SEVI experiment. The solid (dashed) lines indicate the IR (calculated) frequencies for the assigned vibronic levels, corresponding to the values given in Table I. The gray trace in panel III is a close-to-threshold spectrum of peaks G and H, showing the narrower FWHM. For reasons of clarity, not all features are presented with their individual close-to-threshold spectra. Peak B intensity is five times in region I spectrum for clarity.

transition intensities are approximated by comparing lower resolution SEVI spectra that cover the whole energy range with the PE spectra.

Overall, 23 features were observed in the SEVI spectra of C_2H^- in the *e*BE range between 23 000 and 29 650 cm^{-1}. Peak A is the most intense feature in region I of Fig. 2, centered at 23 943 cm^{-1} with a FWHM of 20 cm^{-1}. The features within region II are weaker compared to features observed in the other regions, with widths varying from 50 cm^{-1} (peak C) to 30 cm^{-1} (peak F). Within region III lies the origin of the first excited state of the radical, the $\tilde{A}\,^2\Pi$ state. These features are among the most intense transitions observed in the SEVI study of C_2H^-, and the narrowest. For example, peak G, centered at 27 542 cm^{-1}, has a width of 14 cm^{-1}. Region IV comprises weak and moderately intense transitions. The most intense feature of that region, P, sits at 29 154 cm^{-1} with a width of 12 cm^{-1}.

The SEVI spectra of C_2D^- revealed 19 features in the *e*BE range between 23 500 and 29 500 cm^{-1}. The distribution of peaks within the panels of Fig. 3 is similar to Fig. 2. Peak A, the most intense feature in region I of C_2D, is centered at 23 955 cm^{-1} with a FWHM of 22 cm^{-1}. Region II again contained only weak transitions. Peak C, centered at 25 693 cm^{-1}, has a width of 35 cm^{-1}, and peak F at 26 567 cm^{-1} has a width of 30 cm^{-1}. Region III of Fig. 3

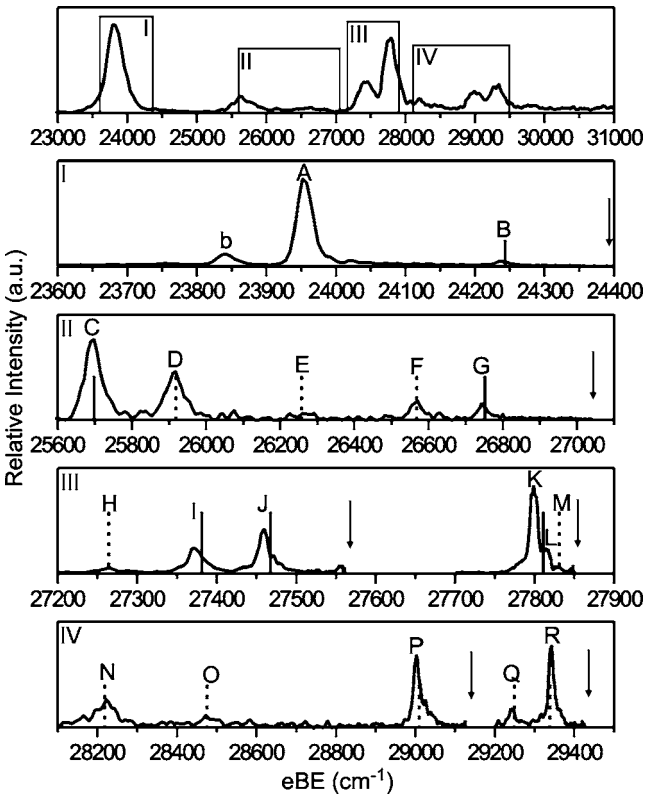

FIG. 3. SEVI spectra of C_2D^- in spectral regions I–IV. Top trace is the PE spectrum recorded by Taylor *et al.* (Ref. 44) at 55° laser polarization, with the corresponding regions I–IV indicated. The arrows indicate photon energies in the SEVI experiment. The solid (dashed) lines indicate the IR (calculated) frequencies for the assigned vibronic levels, corresponding to the values given in Table II. For reasons of clarity, not all features are presented with their individual close-to-threshold spectra.

includes the transition to the origin of the first excited state of C_2D. The peaks in this region are intense, similar to C_2H. Peak K, at 27 799 cm^{-1}, has a FWHM of 11 cm^{-1}. Region IV includes two strong transitions, peaks P and R, with widths of 15–20 cm^{-1}, and several weak peaks that are also broader.

Tables I and II list all the transitions observed in the SEVI spectra of C_2H^- and C_2D^-, and compare them to previous experimental measurements and predictions from recent theoretical work. This comparison is visualized in Figs. 2 and 3, where the solid and dashed vertical lines represent either a previously determined experimental band center or a calculated value. We note that several of the SEVI transitions reported here had not been seen in earlier experiments, particularly for C_2D.

SEVI also provides information on the photoelectron angular distribution (PAD). For one-photon detachment, the PAD is given by[63]

$$\frac{d\sigma}{d\Omega} = \frac{\sigma_{\text{total}}}{4\pi}\left(1 + \beta(e\text{KE})\left(\frac{3}{2}\cos^2(\theta) - \frac{1}{2}\right)\right), \tag{2}$$

where θ is the angle between the direction of the photoelectron ejection and the polarization vector of the incident photon. The anisotropy parameter β lies between 2 and −1, with these limits corresponding to $\cos^2\theta$ and $\sin^2\theta$ distributions, respectively, and provides information on the orbital angular momentum l of the ejected photoelectron; s-wave ($l=0$) detachment leads to $\beta \cong 0$, p-wave to $\beta \cong 2$, and $s+d$ wave to $\beta \cong -1$.

Figure 4 shows the transformed SEVI image of C_2H^- taken at photon energy of 28 183.6 cm^{-1} and a repeller voltage of 350 V, along with the corresponding photoelectron spectrum. It represents a low-resolution, high coverage SEVI spectrum that includes all the transitions in Fig. 2 up to peak L. The PADs for the two most prominent outer rings, features A and C, are peaked along the laser polarization direction, with $\beta=1.9$ and 1.8, respectively, while the PAD for peak G has more intensity perpendicular to the laser polarization direction, with $\beta=-0.3$. The features at smaller radii than peak G are nearly isotropic. These values of β thus indicate that features A and C are dominated by p-wave detachment, while peaks G–L are dominated by s-wave detachment. Tables I and II characterize the PAD of each transition in the SEVI spectrum according to its dominant s or p character; these were extracted from SEVI spectra at a variety of laser wavelengths. Generally, those that have β value greater than 1.5 are labeled as "p," and those with β value less than 0.5 (or slightly negative) are labeled as "s." We find interlaced s and p scatterings for the lower eBE features of both isotopic species, but at higher energy, s-wave detachment dominates. For some of the weak transitions at high eBE, it is difficult to determine whether they are dominated by s-wave or p-wave scattering, so the s/p labeling is left blank.

As discussed in previous work[43,44] and in the next section, the PAD provides insight into vibronic coupling effects in C_2H. However, there is an additional consideration of considerable interest here. According to the Wigner threshold law,[64] the photodetachment cross section σ near threshold is given by

$$\sigma \propto (\Delta E)^{l+0.5}, \tag{3}$$

where $\Delta E=(h\nu-E_{\text{th}})$ is the difference between the photon energy and the detachment threshold. Equation (3) predicts that the cross section drops for small ΔE regardless of l, but this effect is much more pronounced for processes with $l>0$. Consequently, anion ZEKE spectroscopy,[57] which selectively detects electrons produced at values of ΔE of a few cm^{-1}, works only for s-wave detachment. This limitation is significant since many anionic species do not undergo s-wave detachment near threshold owing to symmetry or the nature of the orbital from which detachment occurs.[65] In SEVI, the energy resolution increases with decreasing ΔE, raising the question of whether its high-resolution capabilities can be applied to p-wave detachment.

Figure 5 shows a SEVI image and photoelectron spectra of peaks A and d in C_2H, both of which undergo p-wave detachment, taken at two photon energies (see caption) and a repeller voltage of 150 V. These peaks were partially resolved by Ervin and Lineberger[43] and assigned as the vibrational origin and the $\tilde{X}(0,1,0) \leftarrow \tilde{X}(0,1,0)$ transitions in C_2H. The SEVI spectra here represent much higher resolution conditions than in Fig. 4, with the lower photon energy lying only 310 cm^{-1} above peak A. Each peak has a FWHM of 20–30 cm^{-1} in Fig. 5, and the pair is fully resolved. Figure 5 thus demonstrates for the first time that SEVI can be

TABLE I. Peak positions (cm^{-1}), photoelectron angular momentum (see text), and assignments for the C_2H^- SEVI spectra. The uncertainties in the *e*BE values are ±5–10 cm^{-1} for most transitions; ♦ indicate uncertainties of ±15–25 cm^{-1}; * indicate uncertain assignments.

Peak	*e*BE (cm^{-1})	Offset	PAD[a]	Previous observation (cm^{-1})[b]	Theory (cm^{-1})[c]	Assignment
e	23 711♦	−232	p	[−220]		$\tilde{X}(0,2,0)\leftarrow\tilde{X}(0,2,0)$
d	23 811	−132	p	[−135]		$\tilde{X}(0,1,0)\leftarrow\tilde{X}(0,1,0)$
A	23 943	0	p	[23947]		$\tilde{X}(0,0^0,0)$
B	24 317	374	s	372[d][365]	371	$\tilde{X}(0,1^1,0)$
C	25 805♦	1862	p	1841[e][1850]	1838	$\tilde{X}(0,0^0,1)$
c	25 905♦	1962	s			$\tilde{X}(0,2,1)\leftarrow\tilde{X}(0,1,0)$
D	26 045♦	2102	s	2091[f][2120]	2097	$\tilde{X}(0,1^1,1)$
E	26 115♦	2172	s	2166[d]	2167	$\tilde{X}(0,5^1,0)$
b	26 385♦	2442	p	[2455]		$\tilde{X}(0,3,1)\leftarrow\tilde{X}(0,1,0)$
F	26 874	2931	s	2928[g][2935]	2934	$\tilde{X}(0,3^1,1)$
G	27 542	3599	s	3600[h]	3604	$\tilde{X}(0,1^1,2),\tilde{X}(1,1^1,0),\tilde{A}(0,0,0)^1$
H	27 631	3688	s	3693[i]	3691	$\tilde{X}(1,1^1,0),\tilde{X}(0,1^1,2),\tilde{A}(0,0,0)^1$
I	27 728	3785	s	3786[i]	3791	$\tilde{X}(0,5^1,1),\tilde{A}(0,0,0)^1$
J	27 957	4014	s	4012[i]	4011	$\tilde{X}(0,9^1,0),\tilde{X}(0,5^1,1),\tilde{A}(0,0,0)^1$
K	28 047	4104	s	4108[i]	4094	$\tilde{X}(0,9^1,0),\tilde{A}(0,0,0)^1$
L	28 066	4123	s			
M	28 550♦	4607			4593	$\tilde{X}(0,3^1,2),\tilde{A}(0,0,0)^1$
N	28 845♦	4902			4887	$\tilde{X}(1,4^0,0)^*$
O	28 970♦	5027		5006[j]	5005	$\tilde{X}(0,11^1,0)^*$
P	29 154	5211	s		5222	$\tilde{A}(0,0,1)^1,\tilde{X}(0,1^1,3)$
Q	29 350	5407			5399	$\tilde{X}(1,1^1,1),\tilde{X}(1,5^1,0)$
R	29 382	5439	s		5445	$\tilde{X}(0,5^1,2),\tilde{A}(0,0,1)^1$
S	29 573	5630	s		5630	$\tilde{X}(0,9^1,1),\tilde{A}(0,0,1)^1$

[a]"s" indicates *s*-wave detachment. "p" indicates *p*-wave detachment. Peaks too weak to determine PAD are left blank.
[b]Values in [ ] are from Ref. 43.
[c]Reference 54.
[d]Reference 41.
[e]Reference 30.
[f]Reference 40.
[g]Reference 38.
[h]Reference 31.
[i]Reference 29.
[j]Reference 67.

applied to *p*-wave detachment under conditions that yield substantially better energy resolution than photoelectron spectroscopy.

In the top (lower photon energy) trace of Fig. 5, the relative intensity of peak A compared to peak d is lower than in the bottom trace. This observation can be explained with reference to Eq. (3), according to which

$$\frac{\sigma_A}{\sigma_d}=\left(\frac{\Delta E_A}{\Delta E_d}\right)^{3/2} \tag{4}$$

for *p*-wave detachment, with the result that the ratio of cross sections will decrease as the photon energy is lowered. Hence, although SEVI can be used to measure *p*-wave photodetachment transitions at high resolution, the relative intensities will be quite sensitive to photon energy. This effect will occur much more weakly for *s*-wave transitions since the corresponding exponent is 1/2, not 3/2.

IV. DISCUSSION

Assignments of the peaks in the SEVI spectra are aided by comparison to previously measured vibronic levels and calculated frequencies. Tarroni and Carter[54] have calculated the vibronic levels of C_2H and C_2D with up to 10 000 cm^{-1} of internal energy, and in the process reassigned a few previously observed IR transitions. Assignments of the vibronic species in this paper are based on those reported by Tarroni and Carter[54] and are listed in Tables I and II. The (ν_1,ν_2,ν_3) notation indicates the number of quanta in the C–H stretch, CCH bend, and C–C stretch vibrations, with the superscript indicating vibronic angular momentum. Overall, there is excellent agreement between the SEVI frequencies and previous observations, with most deviations less than 10 cm^{-1}.

Note that Tarroni and Carter[54] have calculated many more levels than we have observed and assigned, and, particularly for the high *e*BE transitions, the correspondence

TABLE II. Peak positions (cm^{-1}), photoelectron angular momentum (see text), and assignments for the C_2D^- SEVI spectra. The uncertainties in the *e*BE values are ±5–10 cm^{-1} for most transitions; ♦ indicate uncertainties of ±15–25 cm^{-1}.

Peak	*e*BE (cm^{-1})	Offset	PAD[a]	Previous observation (cm^{-1})[b]	Theory (cm^{-1})[c]	Assignment
b	23 842	−113	p	[−120]		$\tilde{X}(0,1,0)\leftarrow\tilde{X}(0,1,0)$
A	23 955	0	p	[23979]		$\tilde{X}(0,0^0,0)$
B	24 239	284	s	288[d][270]	287	$\tilde{X}(0,1^1,0)$
C	25 693♦	1738	p	1743[e][1755]	1744	$\tilde{X}(0,0^0,1)$
D	25 912♦	1957	s	[2015]	1963	$\tilde{X}(0,1^1,1)$
E	26 259♦	2304	p		2302	$\tilde{X}(0,2^0,1)$
F	26 567♦	2612	s		2613	$\tilde{X}(0,3^1,1)$
G	26 745	2790	s	2796[f]	2796	$\tilde{X}(1,1^1,0)$
H	27 264	3309	s		3309	$\tilde{X}(0,5^1,1)$
I	27 374	3419	s	3426[g]	3426	$\tilde{X}(1,3^1,0)$
J	27 459	3504	s	3513[h]	3511	$\tilde{X}(0,1^1,2)$
K	27 799	3844	s	3856[g]	3838	$\tilde{A}(0,0,0)^1$
L	27 815	3860	s			
M	27 831	3876			3876	$\tilde{X}(0,11^1,0)$
N	28 216♦	4261	s		4263	$\tilde{X}(0,3^1,2)$
O	28 480♦	4525			4521	$\tilde{A}(0,2,0)^1\mu$
P	29 004	5049	s		5055	$\tilde{X}(0,1^1,3),\tilde{A}(0,0,1)^1$
Q	29 243♦	5288	s		5294	$\tilde{A}(0,4,0)^1\mu$
R	29 342	5387	s		5383	$\tilde{A}(0,0,1)^1$

[a]"s" indicates *s*-wave detachment. "p" indicates *p*-wave detachment. Peaks too weak to determine the PAD are left blank.
[b]Values in [ ] are from Ref. 43.
[c]Reference 54.
[d]Reference 18.
[e]Reference 34.
[f]Reference 37.
[g]Reference 31.
[h]Reference 36.

with theory is not always obvious from the energetics alone. The vibronic symmetry of the neutral state is very useful in this regard. The ethynyl anion is linear with a $^1\Sigma^+$ ground state ($\cdots 4\sigma^2 1\pi^4 5\sigma^2$), and photodetachment to the $\tilde{X}\,^2\Sigma^+$ and $\tilde{A}\,^2\Pi$ states involves ejection from the 5σ and 1π orbitals, respectively. As a result, transitions from the $\tilde{X}(0,0,0)$ level of the anion, which has Σ^+ vibronic symmetry and total vibrational angular momentum of zero, are generally only allowed to neutral levels with either Σ^+ or Π vibronic symmetry with even quanta of total vibrational angular momentum. Transitions to Δ, Φ, etc., vibronic levels are nominally forbidden, so calculated levels with those vibronic symmetries can be eliminated from consideration.

Given that photodetachment to the $\tilde{X}\,^2\Sigma^+$ and $\tilde{A}\,^2\Pi$ states involves ejection from σ and π orbitals, respectively, one expects different PADs for transitions to the two neutral states. The PE spectra of Ervin and Lineberger[43] and Taylor *et al.*[44] showed that photodetachment to the $\tilde{X}\,^2\Sigma^+$ state yielded *p*-wave detachment when $\Delta\nu_2$ is even and *s*-wave detachment when odd, and transitions to pure or mixed $\tilde{A}\,^2\Pi$ levels exhibited *s*-wave detachment. These trends, discussed in more detail below, also hold true for the considerably larger number of transitions seen in the SEVI spectra.

In region I, peak A in both C_2H^- and C_2D^- spectra is assigned to the $^1\Sigma^+$-$^2\Sigma^+$ 0-0 origin band. This assignment gives the electron affinity (EA) of 23 946±10 cm^{-1} (2.9689±0.0011 eV) for C_2H, similar to the previously reported EA of 2.969±0.006 eV.[43] Similarly, EA(C_2D) =23 955±10 cm^{-1} (2.9700±0.0011 eV), only slightly blue-shifted from C_2H and similar to the previously reported EA of 2.973±0.006 eV.[43] For each isotopomer, panel I also shows sequence band transitions from excited bending levels of the anion [i.e., the $\tilde{X}(0,1,0)\leftarrow\tilde{X}(0,1,0)$ and $\tilde{X}(0,2,0)\leftarrow\tilde{X}(0,2,0)$ transitions for C_2H and $\tilde{X}(0,1,0)\leftarrow\tilde{X}(0,1,0)$ for C_2D], labeled with lowercase letters. As shown explicitly in Fig. 5, the origin and sequence-band transitions exhibit strongly positive β values characteristic of *p*-wave scattering.

Peak B, a small feature lying 374 cm^{-1} above the origin transition in C_2H and 284 cm^{-1} in C_2D, is assigned to the transition from the anion ground state to the fundamental bend vibration of the radical ground state, $\tilde{X}(0,1^1,0)$. As discussed previously,[43] an odd $\Delta\nu$ transition in a non-totally symmetric vibration is nominally forbidden in one-photon photoelectron spectroscopy. However, this neutral level has Π vibronic symmetry. It is thus coupled by pseudo-Jahn-

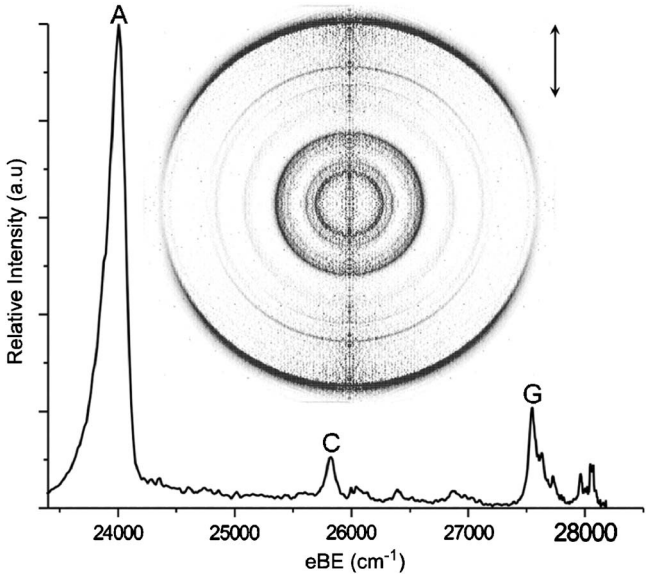

FIG. 4. Inverse-Abel transformed SEVI image of C_2H^- taken at 28 183.6 cm^{-1} and 350 V VMI repeller voltage, and its angular integration plotted against *e*BE. Different angular distributions can be seen for different transitions.

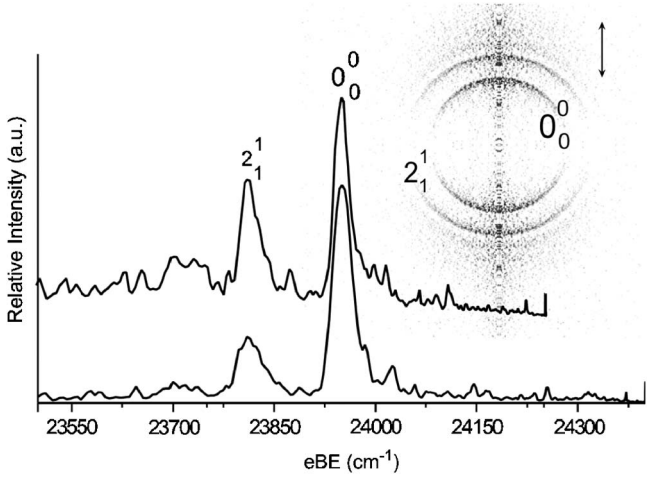

FIG. 5. Inverse-Abel transformed SEVI image of C_2H origin transition, recorded with photon energy of 24 253.4 cm^{-1} and VMI voltage of 150 V. The angular integration of the image, as well as the integration of the image taken at 24 407.5 cm^{-1} and 150 V, is also presented. The falling cross section as photon energy decreases can be seen in the relative intensities in the spectra.

Teller interaction to the totally symmetric vibrational levels of the $\tilde{A}$ state, which also have Π vibronic symmetry, resulting in nonzero intensity in the photoelectron spectrum. Explicit evidence of this coupling is seen in the PAD, which shows the *s*-wave detachment characteristic of a transition to the $\tilde{A}$ state.

Region II comprises several fairly weak transitions to excited vibrational levels of the $\tilde{X}$ state. Peak C is assigned to $\tilde{X}(0,0^0,1)$ for both isotopes. This $\Delta\nu=1$ transition in the totally symmetric C–C stretching vibration is allowed in one-photon photodetachment process. Its *p*-wave PAD is in accordance with a transition to a neutral $\tilde{X}$ state level with Σ^+ vibronic symmetry. Peaks D and F in region II have the same vibronic assignments in both isotopes, involving the combination bands of the bend vibration and the C–C stretching vibration. The very weak peak E, however, is assigned to the $\tilde{X}(0,5^1,0)$ level in C_2H and the $\tilde{X}(0,2^0,1)$ level in C_2D; the corresponding peaks for the other isotopic species are missing because of the low intensities of these transitions. Region II in part overlaps with the PE spectrum acquired by Ervin and Lineberger,[43] and a comparison between the two shows fewer transitions in the SEVI spectra. For example, transitions to the $\tilde{X}(0,2^0,0)$ and $\tilde{X}(0,3^1,0)$ states are not seen in the SEVI spectra. These are examples of weak transitions at slightly higher *e*BE than a strong transition (the origin band in this case) that are, in general, difficult to observe in the transformed image because they occur on top of the signal from the strong transition in the raw image.

Region III covers the spectral region of the $\tilde{A}$ state origin. The PE spectrum of this region recorded by Taylor *et al.*[44] was somewhat problematic in terms of spectral assignment. For both isotopic species, one of the two intense peaks was assigned to the $\tilde{A}(0,0,0)^1$ state, but the second peak, at higher *e*BE, appeared to match the energy of the forbidden photodetachment transition from the anion ground state to the neutral $\tilde{A}(0,1,0)^0$ state with Σ^- vibronic symmetry. The higher resolution SEVI spectra show that the two peaks in region III of the PE spectrum split into multiple features, G–L in C_2H and H–L in C_2D, each of which lies at or near an allowed photodetachment transition that has been identified experimentally by infrared spectroscopy. We can thus revise the problematic assignment of the photoelectron spectrum with the new assignments in Tables I and II.

In Table I, the assignments of the spectral features in this region are all given as admixtures of excited vibrational levels of the $\tilde{X}\,^2\Sigma^+$ state with the $\tilde{A}(0,0,0)^1$ level, while in Table II, for C_2D, peaks G–J are listed as pure $\tilde{X}$ state levels with Π vibronic symmetry and peak K is given as the $\tilde{A}(0,0,0)^1$ level with no admixture of $\tilde{X}$ state levels. This distinction, made by Tarroni and Carter[54] is based on calculation of the mixing coefficients as well as the calculated and experimental[29,31] spin-orbit splittings for the levels in question; the latter are obtained from rotationally resolved IR spectra. A pure $^2\Sigma^+$ level has no spin-orbit splitting, while a pure $\tilde{A}\,^2\Pi$ level of C_2H is estimated[31] to have a spin-orbit splitting of around -25 cm^{-1}. In C_2H, the IR experimental spin-orbit splittings for bands G–K vary from -2.2 cm^{-1} (peak J) to -7.1 cm^{-1} (peak G), supporting the assignment of each band to an $\tilde{X}+\tilde{A}$ admixture. In C_2D, on the other hand, band K has a spin-orbit splitting of -11.2 cm^{-1}, considerably larger than all the nearby bands, and that is why it is assigned as the "unique" $\tilde{A}(0,0,0)^1$ level. This assignment is an approximation, since its spin-orbit splitting is only about half of the expected value for a pure $\tilde{A}$ state level. Bands I and J have nonzero spin-orbit splittings of -2.2 and -6.6 cm^{-1}, and H has calculated spin-orbit splitting of -0.5 cm^{-1}; all are smaller than for band K but nonzero, indicating some mixing with the $\tilde{A}$ state.

The SEVI spectra offer a complementary view of vi-

bronic coupling in region III. All bands in this region for both isotopic species undergo *s*-wave detachment, which, as discussed above, indicates detachment to a neutral level with at least some $\tilde{A}$ state character. However, the intensity patterns are quite different for the two isotopic species, with peak G the most intense for C_2H and peak K the most intense for C_2D. In fact, the SEVI intensities approximately track the spin-orbit splittings, with the most intense peaks corresponding to those levels with the largest spin-orbit splitting. This correlation suggests that the intensities in the SEVI spectra reflect the extent of $\tilde{A}$ state mixing, a perfectly reasonable result since the anion ground vibrational state has good Franck-Condon overlap with the $\tilde{A}(0,0,0)^1$ level but zero overlap with odd bending levels of the $\tilde{X}$ state.

Peaks K and L are split by only 19 cm^{-1} for C_2H and 16 cm^{-1} for C_2D, whereas both theory[54] and IR spectroscopy[29,31] indicate that there is only one allowed vibronic level in the vicinity of each pair of peaks. The experimental band centers for this level fall between K and L for both isotopic species, raising the question of whether K and L represent two distinct vibronic transitions or are components of a single transition. In C_2H, the closest vibronic level above the one assigned to K is the $\tilde{A}(0,1,0)^0$ level with Σ^- vibronic symmetry at 4143 cm^{-1}. This level lies 20 cm^{-1} above peak L. However, as pointed out above, photodetachment to this level is forbidden. Moreover, the corresponding level in C_2D is at 4017 cm^{-1}, well above peaks K and L in the C_2D^- SEVI spectrum. It thus appears that we can rule out this level as being responsible for peak L. In C_2D, the closest allowed vibronic level to the K and L pair is assigned to peak M in the SEVI spectrum.

Therefore, it appears that there is no obvious way to assign peaks K and L to two vibronic transitions, suggesting that they are components of the same transition. One way this might come about is if K and L each represented a group of unresolved rotational transitions associated with a single vibronic transition. Indeed, the IR spectra (taken at room temperature) from the $\tilde{X}(0,0^0,0)$ state to the upper state responsible for peak K shows the characteristic complicated rotational and spin-orbit structure associated with $^2\Pi$-$^2\Sigma^+$ transitions and is spread over more than 30 cm^{-1}.[29,31] When we simulated the rotational structure for photodetachment from the C_2H^- anion[66] and convoluted the result with our experimental resolution, we found that the six branches added up to form a rotational profile with a single peak at the center. However, in C_2H, peak L appears as a well separated feature of similar intensity as peak K. While the IR spectra for C_2H from transitions to many other excited states show rotational profiles similar to those for state K, none of the other SEVI peaks split into two features even under similar high-resolution conditions. In C_2D, peak L, a shoulder on peak K, is spaced from peak K by approximately the spin-orbit splitting of that vibronic state, −11 cm^{-1}.[31] This is not the case in C_2H, where the spin-orbit splitting is much smaller, −3 cm^{-1} for peak K,[29] but the spacing between peaks K and L is larger. Hence, the origin of the splitting between K and L in C_2H is not obvious at this time.

Region IV in Figs. 2 and 3 contain a mixture of vibrations from the ground state and the first excited states in C_2H and C_2D. Many of these high energy vibronic levels were observed for the first time in a gas phase experiment. In the C_2H^- spectra, the narrow peak P is assigned to transition to the $\tilde{A}(0,0,1)^1$, $\tilde{X}(0,1^1,3)$ vibronic level. The other narrow peaks, R and S, also correspond to vibronic levels with $\tilde{A}(0,0,1)^1$ character. On the other hand, peaks N, O, and Q, assigned to excited vibrational levels on the $\tilde{X}$ state, are comparably much weaker and broader. This intensity behavior is similar to the $\tilde{A}(0,0,0)^1$ levels discussed earlier. Region IV in the C_2D^- spectra contains mainly transitions to vibronic levels with $\tilde{A}$ state characteristic, with only peak N assigned to an $\tilde{X}$ state vibration. Peaks P and R, assigned to vibronic levels with $\tilde{A}(0,0,1)^1$ characteristics, are again the strongest transitions in this region. The most likely assignments for the observed peaks in this region are listed in Tables I and II, a few with asterisks to indicate uncertain assignments due to multiple close-lying vibronic levels.

V. CONCLUSIONS

SEVI spectra of the ethynyl and ethynyl-*d* anions are reported, resolving numerous features associated with photodetachment to the $\tilde{X}\,^2\Sigma^+$ and $\tilde{A}\,^2\Pi$ states that were not observed in previous anion photoelectron spectra,[43,44] as well as clarifying past problematic assignments. Detailed assignments were carried out based on observed IR frequencies, calculated vibronic levels, and the photoelectron anisotropy parameter of the observed transitions. Several higher-lying vibronic levels of C_2H and C_2D were seen here experimentally for the first time. The spectra yield new insights into the vibronic coupling between the $\tilde{X}$ and $\tilde{A}$ states near the $\tilde{A}$ state origin, with the intensities in this spectral region indicating the degree of $\tilde{A}$ state character for each neutral vibronic level. Finally, we showed that SEVI can be applied to transitions involving pure *p*-wave detachment, even though the cross section for *p*-wave detachment is very low close to threshold. This result bodes well for the generality of SEVI, since nearly all anions undergo either *s*-wave or *p*-wave photodetachment near threshold.

ACKNOWLEDGMENTS

One of the authors (D.M.N.) acknowledges support from the Air Force Office of Scientific Research under Grant No. F49620-03-1-0085. Another author (E.G.) thanks the Natural Science and Engineering Research Council of Canada for a postgraduate scholarship.

[1] A. Osterwalder, M. J. Nee, J. Zhou, and D. M. Neumark, J. Chem. Phys. **121**, 6317 (2004).
[2] K. D. Tucker, M. L. Kutner, and P. Thaddeus, Astrophys. J. **193**, L115 (1974).
[3] A. Wootten, E. P. Bozyan, D. B. Garrett, R. B. Loren, and R. L. Snell,Astrophys. J. **239**, 844 (1980).
[4] W. M. Irvine, M. Ohishi, and N. Kaifu, Icarus **91**, 2 (1991).
[5] A. Dutrey, S. Guilloteau, and M. Guelin, Astron. Astrophys. **317**, L55 (1997).
[6] R. Lucas and H. S. Liszt, Astron. Astrophys. **358**, 1069 (2000).
[7] T. I. Hasegawa and S. Kwok, Astrophys. J. **562**, 824 (2001).
[8] D. Teyssier, D. Fosse, M. Gerin, J. Pety, A. Abergel, and E. Roueff,

Astron. Astrophys. **417**, 135 (2004).
[9] J. H. Kiefer and W. A. Vondrasek, Int. J. Chem. Kinet. **22**, 747 (1990).
[10] J. H. Kiefer, S. S. Sidhu, R. D. Kern, K. Xie, H. Chen, and L. B. Harding, Combust. Sci. Technol. **82**, 101 (1992).
[11] W. Boullart, K. Devriendt, R. Borms, and J. Peeters, J. Phys. Chem. **100**, 998 (1996).
[12] E. L. Cochran, F. J. Adrian, and V. A. Bowers, J. Chem. Phys. **40**, 213 (1964).
[13] W. R. M. Graham, K. I. Dismuke, and W. Weltner, J. Chem. Phys. **60**, 3817 (1974).
[14] M. Jinguji, C. A. McDowell, and K. Shimokoshi, J. Mol. Struct. **130**, 317 (1985).
[15] R. J. Saykally, L. Veseth, and K. M. Evenson, J. Chem. Phys. **80**, 2247 (1984).
[16] J. M. Brown and K. M. Evenson, J. Mol. Spectrosc. **131**, 161 (1988).
[17] C. Pfelzer, M. Havenith, M. Peric, P. Murtz, and W. Urban, J. Mol. Spectrosc. **176**, 28 (1996).
[18] C. Schmidt, M. Peric, P. Murtz, M. Wienkoop, M. Havenith, and W. Urban, J. Mol. Spectrosc. **190**, 112 (1998).
[19] K. Sastry, P. Helminger, A. Charo, E. Herbst, and F. C. Delucia, Astrophys. J. **251**, L119 (1981).
[20] C. A. Gottlieb, E. W. Gottlieb, and P. Thaddeus, Astrophys. J. **264**, 740 (1983).
[21] M. Bogey, C. Demuynck, and J. L. Destombes, Astron. Astrophys. **144**, L15 (1985).
[22] Y. Endo, H. Kanamori, and E. Hirota, Chem. Phys. Lett. **160**, 280 (1989).
[23] H. S. P. Muller, T. Klaus, and G. Winnewisser, Astron. Astrophys. **357**, L65 (2000).
[24] M. E. Jacox, Chem. Phys. **7**, 424 (1975).
[25] M. E. Jacox and W. B. Olson, J. Chem. Phys. **86**, 3134 (1987).
[26] R. A. Shepherd and W. R. M. Graham, J. Chem. Phys. **86**, 2600 (1987).
[27] D. Forney, M. E. Jacox, and W. E. Thompson, J. Mol. Spectrosc. **170**, 178 (1995).
[28] P. G. Carrick, A. J. Merer, and R. F. Curl, J. Chem. Phys. **78**, 3652 (1983).
[29] R. F. Curl, P. G. Carrick, and A. J. Merer, J. Chem. Phys. **82**, 3479 (1985).
[30] H. Kanamori, K. Seki, and E. Hirota, J. Chem. Phys. **87**, 73 (1987).
[31] W. B. Yan, C. B. Dane, D. Zeitz, J. L. Hall, and R. F. Curl, J. Mol. Spectrosc. **123**, 486 (1987).
[32] W. B. Yan, J. L. Hall, J. W. Stephens, M. L. Richnow, and R. F. Curl, J. Chem. Phys. **86**, 1657 (1987).
[33] H. Kanamori and E. Hirota, J. Chem. Phys. **89**, 3962 (1988).
[34] H. Kanamori and E. Hirota, J. Chem. Phys. **88**, 6699 (1988).
[35] K. Kawaguchi, T. Amano, and E. Hirota, J. Mol. Spectrosc. **131**, 58 (1988).
[36] J. W. Stephens, W. B. Yan, M. L. Richnow, H. Solka, and R. F. Curl, J. Mol. Struct. **190**, 41 (1988).
[37] W. B. Yan, H. E. Warner, and T. Amano, J. Chem. Phys. **94**, 1712 (1991).
[38] W. B. Yan and T. Amano, J. Chem. Phys. **99**, 4312 (1993).
[39] M. Vervloet and M. Herman, Chem. Phys. Lett. **144**, 48 (1988).
[40] Y. C. Hsu, J. J. M. Lin, D. Papousek, and J. J. Tsai, J. Chem. Phys. **98**, 6690 (1993).
[41] Y. C. Hsu, Y. J. Shiu, and C. M. Lin, J. Chem. Phys. **103**, 5919 (1995).
[42] W. Y. Chiang and Y. C. Hsu, J. Chem. Phys. **111**, 1454 (1999).
[43] K. M. Ervin and W. C. Lineberger, J. Phys. Chem. **95**, 1167 (1991).
[44] T. R. Taylor, C. S. Xu, and D. M. Neumark, J. Chem. Phys. **108**, 10018 (1998).
[45] H. Thummel, M. Peric, S. D. Peyerimhoff, and R. J. Buenker, Z. Phys. D: At., Mol. Clusters **13**, 307 (1989).
[46] M. Peric, R. J. Buenker, and S. D. Peyerimhoff, Mol. Phys. **71**, 673 (1990).
[47] M. Peric, S. D. Peyerimhoff, and R. J. Buenker, Mol. Phys. **71**, 693 (1990).
[48] M. Peric, B. Engels, and S. D. Peyerimhoff, J. Mol. Spectrosc. **150**, 56 (1991).
[49] M. Peric, B. Engels, and S. D. Peyerimhoff, J. Mol. Spectrosc. **150**, 70 (1991).
[50] M. Peric, S. D. Peyerimhoff, and R. J. Buenker, J. Mol. Spectrosc. **148**, 180 (1991).
[51] M. Peric, W. Reuter, and S. D. Peyerimhoff, J. Mol. Spectrosc. **148**, 201 (1991).
[52] M. Peric, S. D. Peyerimhoff, and R. J. Buenker, Z. Phys. D: At., Mol. Clusters **24**, 177 (1992).
[53] S. Carter, N. C. Handy, C. Puzzarini, R. Tarroni, and P. Palmieri, Mol. Phys. **98**, 1697 (2000).
[54] R. Tarroni and S. Carter, J. Chem. Phys. **119**, 12878 (2003).
[55] R. Tarroni and S. Carter, Mol. Phys. **102**, 2167 (2004).
[56] K. R. Asmis, T. R. Taylor, and D. M. Neumark, J. Chem. Phys. **111**, 8838 (1999).
[57] T. N. Kitsopoulos, I. M. Waller, J. G. Loeser, and D. M. Neumark, Chem. Phys. Lett. **159**, 300 (1989).
[58] M. J. Nee, A. Osterwalder, J. Zhou, and D. M. Neumark, J. Chem. Phys. **125**, 014306 (2006).
[59] J. Zhou, E. Garand, W. Eisfeld, and D. M. Neumark, J. Chem. Phys. **127**, 034304 (2007).
[60] A. T. J. B. Eppink and D. H. Parker, Rev. Sci. Instrum. **68**, 3477 (1997).
[61] U. Even, J. Jortner, D. Noy, N. Lavie, and C. Cossart-Magos, J. Chem. Phys. **112**, 8068 (2000).
[62] D. W. Chandler and P. L. Houston, J. Chem. Phys. **87**, 1445 (1987).
[63] J. Cooper and R. N. Zare, J. Chem. Phys. **48**, 942 (1968).
[64] E. P. Wigner, Phys. Rev. **73**, 1002 (1948).
[65] K. J. Reed, A. H. Zimmerman, H. C. Anderson, and J. I. Brauman, J. Chem. Phys. **64**, 1368 (1976).
[66] S. Brunken, C. A. Gottlieb, H. Gupta, M. C. McCarthy, and P. Thaddeus, Astron. Astrophys. **464**, L33 (2007).
[67] Y. C. Hsu, F. T. Chen, L. C. Chou, and Y. J. Shiu, J. Chem. Phys. **105**, 9153 (1996).